Solidification Sequence of Spray-Formed Steels

GUILHERME ZEPON, NILS ELLENDT, VOLKER UHLENWINKEL, and CLAUDEMIRO BOLFARINI

Solidification in spray-forming is still an open discussion in the atomization and deposition area. This paper proposes a solidification model based on the equilibrium solidification path of alloys. The main assumptions of the model are that the deposition zone temperature must be above the alloy's *solidus* temperature and that the equilibrium liquid fraction at this temperature is reached, which involves partial remelting and/or redissolution of completely solidified droplets. When the deposition zone is cooled, solidification of the remaining liquid takes place under near equilibrium conditions. Scanning electron microscopy (SEM) and optical microscopy (OM) were used to analyze the microstructures of two different spray-formed steel grades: (1) boron modified supermartensitic stainless steel (SMSS) and (2) D2 tool steel. The microstructures were analyzed to determine the sequence of phase formation during solidification. In both cases, the solidification model proposed was validated.

DOI: 10.1007/s11661-015-3253-1

I. INTRODUCTION

IN the spray-forming process, a molten metal is gas atomized to produce a spray cone composed of droplets with diameters ranging from 10 to 500 μm, which impact a substrate with velocities of up to 100 to 200 ms^{-1} with a distribution of fully liquid, partially solidified, and completely solidified droplets.[1] Before they reach the substrate, the metal droplets are cooled at high rates, ranging typically from 10^2 to 10^5 Ks^{-1}. When the droplets are deposited onto the substrate, solidification continues in the deposition zone and a solid, dense, and homogeneous deposit is formed.[2] Several types of alloys such as steels, cast irons, Ni-alloys, Al-alloys, and Cu-alloys, as well as different geometries (billets, tubes, and rings) have been successfully produced by spray-forming.[3–14] In all cases, the spray-formed microstructures present noticeable features: (1) equiaxed grains with diameters from 10 to 50 μm; (2) a high level of microstructural homogeneity and macrosegregation free; (3) uniform and homogeneous distribution of eutectic and second phases. The advantageous microstructure produced by the spray-forming process is well-known from research; however, solidification at the deposition zone and the creation of such a characteristic microstructure are still an open discussion. How the microstructure of the droplets (usually columnar/dendritic) that impact the deposition zone completely solidified turns into the equiaxed microstructure of spray-formed deposits, is not yet well explained nor understood.

Different solidification models to explain the generation of the equiaxed grains in spray deposited alloys have been reported in the literature.[15–17] The first one was called the dendrite arm fragmentation model.[15] This early model argues that dendritic arms present in the partially solidified droplets are extensively fragmented because of (1) the mechanical forces produced by the impact of the droplets on the deposition zone; and (2) the shear stresses induced by the turbulent fluid convection in the deposition zone. Such dendrite fragments become potent nuclei for solidification, which grow and generate the equiaxed grains microstructure. Subsequently, Grant[16] proposed that the deposition zone must have an equilibrium temperature above the *solidus* temperature, which is constant during the deposition process. Consequently, part of the solid fraction of the droplets is remelted in the deposition zone in order to reach the equilibrium liquid fraction. According to the author, the significant liquid fraction and the temperature gradient present in the deposition zone facilitate the spheroidization of the remaining solid fragments in an attempt to minimize the solid/liquid interfacial area. Although this model is well-supported by theoretical aspects, an experimental validation was missing. For instance, no measurements of the equilibrium temperature were presented and only microstructures with considerable grain coarsening after solidification were shown.

Recently, Henein[17] argued that solidification must occur in discrete regions and that there cannot be any liquid merging between adjacent droplets at the deposition zone. The argument is based on the fact that the same eutectic fraction (lower than the equilibrium fraction) was observed both in the impulse atomized droplets and in the deposit formed by impulse spray of

GUILHERME ZEPON, Ph.D. Student, is with the Post-Graduation Program of Materials Science and Engineering (PPG-CEM), Federal University of São Carlos (UFSCar), Rod. Washington Luiz, Km 235, São Carlos, SP 13565-905, Brazil. Contact e-mail: guizepon@yahoo.com.br NILS ELLENDT, Post-Doctoral Research Engineer, and VOLKER UHLENWINKEL, Researcher Head of Spray Forming, are with the Foundation Institute of Materials Science (IWT), Badgasteiner Str. 3, 28359 Bremen, Germany. CLAUDEMIRO BOLFARINI, Titular Professor, is with the Materials Engineering Department, Federal University of São Carlos (UFSCar).

Manuscript submitted April 14, 2015.
Article published online November 25, 2015

the Al-0.61 wt pctFe alloy. The lower eutectic fraction suggests that eutectic undercooling is taking place. The author suggests that when the droplets are atomized, they are covered by a nano-thick oxide coating which is not broken when the droplets impact the deposition zone, preserving what the author calls the "droplet region". According to the author, solidification at the deposition zone of the "droplet regions" continues independently of the solute in adjacent "droplet regions". When the deposit cools further, each "droplet region" must nucleate its own second phase, achieving the same fraction of eutectic as the atomized droplets. However, the formation of the nano-thick oxide layer was not experimentally validated. Moreover, this model does not explain the formation of the equiaxed grains characteristic of spray-formed alloys.

In this paper two steel grades were spray-formed: (1) 3kg deposits of boron modified supermartensitic stainless steel (SMSS), with 0.3 and 0.7 wt pct of boron, were spray-formed using laboratory-scale equipment; and (2) billets of D2 tool steel with approximately 100 kg were spray-formed using an equipment with industrial features. The comparison between the microstructures of the spray-formed steels and the overspray powders, as well as the surface temperature measurements were used to track the solidification path of both alloys. Based on the results, a model for the solidification sequence of steels in spray-forming, which considers that conditions close to equilibrium must be attained at the deposition zone, is proposed. Based on the results, a model is proposed for the solidification sequence of steels in spray-forming, which considers that conditions close to equilibrium must be attained at the deposition zone.

A. *Design of Experiment*

Supermartensitic stainless steel modified with 0.3 and 0.7 wt pct of boron (hereinafter named SM-0.3B and SM-0.7B, respectively) were spray-formed using a close-coupled atomizer attached to laboratory-scale equipment. The billet of D2 tool steel was spray-formed at the spray-forming plant at IWT Bremen. The chemical compositions of both alloys are presented in Table I and a summary of the processing parameters used is shown in Table II.

Samples of the spray-formed alloys and of the overspray powders were grinded and polished using conventional metallography procedures. The samples of SM-0.3B and SM-0.7B were etched with $3HCl:1HNO_3$. The boride morphologies were revealed using a deep etching procedure with 10 mL HCl, 3 ml HNO_3, 5 mL $FeCl_3$, and 82 mL ethyl alcohol solution. The D2 samples were etched with 2 pct Nital. The phase identification was performed by X-ray diffraction (XRD) using a Rigaku diffractometer equipped with a Cu tube and a graphite monochromator operating at 40 kV and 40 mA. The microstructures were observed by optical microscopy (OM) and scanning electron microscopy (SEM) using a FEI Inspect S50 Scanning Electron Microscope.

II. RESULTS

A. *Boron Modified Supermartensitic Stainless Steel*

The boron modified supermartensitic stainless steels have some features, which are worth pointing out:

1. Boron has a very limited solubility in steel (<0.008 wt pct), even at the high temperature austenite phase.[18]
2. The presence of boron in the steel composition leads to the formation of M_2B borides (where M = Fe, Cr, Ni, Mo).
3. Both alloys, SM-0.3B and SM-0.7B, have hypoeutectic compositions where the equilibrium solidifi-

Table I. Chemical Composition of the Spray-Formed Alloys

Wt Percent	Pct C	Pct Cr	Pct Ni	Pct Mo	Pct B	Pct Ti	Pct Mn	Pct V	Pct S	Pct Fe
SM-0.3B	0.066	12.00	5.68	2.09	0.37	0.044	0.40	—	0.0014	bal.
SM-0.7B	0.096	11.88	5.88	2.09	0.69	0.041	0.49	—	0.0017	bal.
D2	1.52	11.50	0.27	0.75	—	0.001	0.30	0.91	0.0004	bal.

Table II. Summary of the Processing Parameters Used

Alloy	SM-0.3B	SM-0.7B	D2
Melt atmosphere	argon protection	argon protection	vacuum/argon
Atomization gas	nitrogen	nitrogen	nitrogen
Feedstock mass (kg)	4	4	121
Melt superheat (K)	—	—	150
Pouring temperature K (°C)	1923 (1650)	1923 (1650)	1793 (1520)
Mass flow (kg/s)	0.13	0.13	0.29
GMR	0.62	0.62	1.03
Total atomization time (s)	30	30	424
Atomizer scan angle (deg)	0	0	±4
Scan frequency (Hz)	–	–	15
Spraying distance (mm)	460	460	435
Substrate material	mild steel	mild steel	mild steel

cation path follows the sequence: solidification of γ-Fe as primary phase followed by the eutectic reaction $L \rightarrow M_2B + \gamma\text{-Fe}$.[19]

4. The limited solubility of boron in the steel matrix does not allow the M_2B type borides to be dissolved, which means that the borides are present in the as-solidified microstructure.

It is also important to point out that after solidification the austenite is transformed into martensite, even at low cooling rates, for instance, when the deposit is air cooled inside the spray chamber. However, such solid state transition has no effect on the understanding of solidification in the spray-forming process.

Figure 1 shows the SM-0.3B and SM-0.7B spray-formed deposits. Both disk-shaped deposits are 250 mm in diameter and 15 mm in thickness with a very homogeneous and uniform microstructure. Porosity levels, measured by area fraction, lower than 1 pct were measured in both deposits. Figure 2(a) shows the microstructure of an SM-07.B overspray particle with a diameter of about 200 μm. The particle microstructure is composed of a dendritic martensitic matrix with M_2B borides present in the eutectic constituent between the interdendritic arms. Observe the identification of phases in the XRD presented in Figure 3. The high cooling rates promoted by the gas atomization led to a very refined powder microstructure, in this case with average secondary dendrite arm spacing about 2.5 μm. As demonstrated by Grant,[16] droplets larger than 200 μm are expected to reach the substrate still fully liquid under conventional spray-forming conditions. Therefore, the droplets that land on the deposition zone completely solidified (usually droplet size <50 μm) were cooled at higher rates than the 200 μm droplets, resulting in a more refined microstructure. Figure 2(b) shows the microstructure of a 50 μm diameter droplet. It can be clearly seen that the microstructure is still dendritic, but strongly finer than the one presented in the 200 μm droplet, making it difficult to measure the secondary dendrite arm spacing. Figures 4(a) and (b) present the microstructure of the SM-0.7B spray-formed deposit at two different magnifications. One can see that the spray-formed microstructure consists of equiaxed martensitic grains with M_2B borides present around the grain boundaries (the identification of phases is also presented in Figure 3). The average grain size is around 15 μm, which is much coarser than the powder microstructures. The M_2B borides present in the spray-formed microstructure are also considerably coarser than in the overspray droplets. The microstructure of the borides can be better observed in the SEM images present in Figures 5(a) and (b). No remnants of the dendritic microstructures from the completely solidified droplets are present in the spray-formed microstructure. As pointed out before, the borides after solidification cannot be dissolved in the steel matrix due to the very limited solubility of boron. Based on this, the only possible explanation for the disappearance of the droplet microstructure in the final spray-formed deposit is the remelting and/or redissolution of the borides present in the interdendritic arm spaces at the deposition zone. As shown in Figure 5 (b), the M_2B borides appear in the SM-0.7B spray-formed deposit as a continuous eutectic network interconnected along the microstructure. This result reveals that during the later stages of solidification the liquid at the deposition zone must be continuous, and when the eutectic constituent is

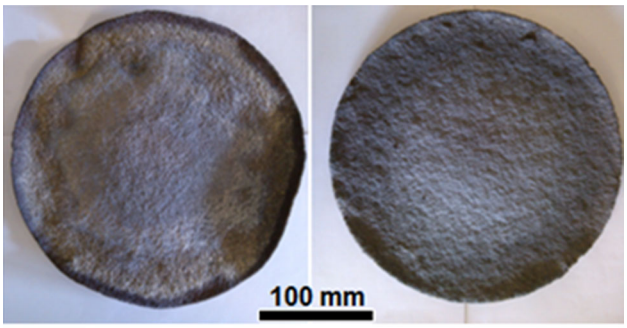

Fig. 1—Spray-formed disks of (*a*) SM-0.3B and (*b*) SM-0.7B.

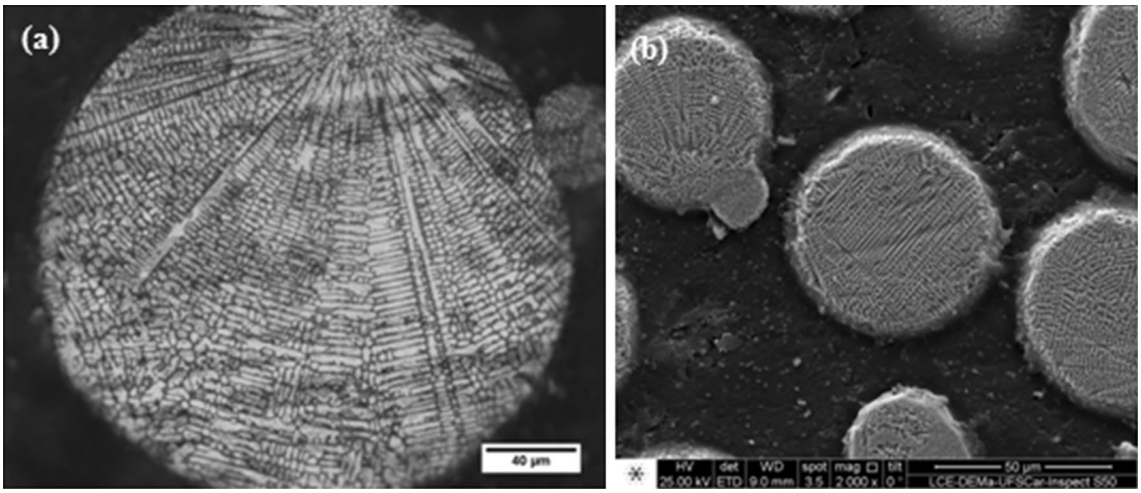

Fig. 2—Microstructure of the overspray powder of SM-0.7B with (*a*) 200 μm (OM) and (*b*) 50 μm (SEM).

solidified no "droplet regions" remain. It is worth stressing that as the borides were solidified at the grain boundaries, no further grain growth was possible after the solidification. Hence, this microstructure is identical to the as-solidified structure (despite the martensitic transformation).

Figure 6(a) shows the microstructure of the SM-0.3B. In this case, the equiaxed grain size is about 35 μm (compared to 15 μm for the SM-0.7B) and the fraction of M_2B borides is considerably smaller. Moreover, some grains are larger than 50 μm, which is larger than the droplet size expected to land completely solidified on the deposition zone. This result also suggests that the completely solidified droplets were partially remelted and/or redissolved within deposition zone. Figure 6(b) shows that even in small amounts, the M_2B borides are still present as an interconnected eutectic network, showing that no "droplets region" was preserved.

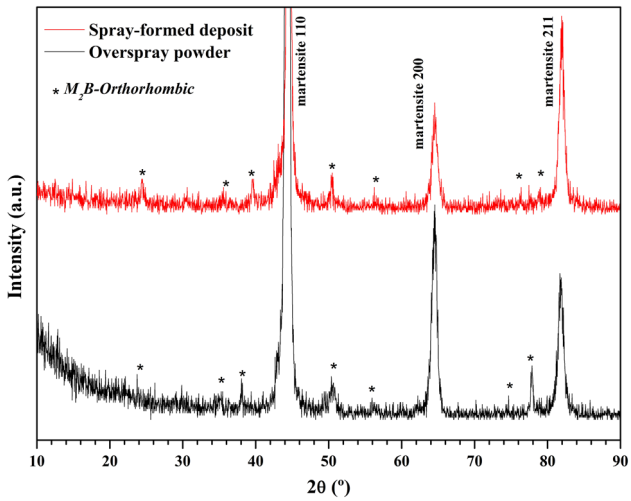

Fig. 3—XRD patterns showing the phases present in the overspray powder and in the spray-formed deposit of SM-0.7B.

B. *D2 Steel*

D2 tool steel is a 12 wt pctCr and 1.5 wt pctC steel with a high hardness derived from the presence of hard carbides such as M_7C_3 in the microstructure. Unlike boron, carbon has considerable solubility in austenite. Figure 7 presents a calculated pseudo-binary phase diagram of D2 steel showing that the equilibrium solidification path (at 1.5 wt pct C) is the formation of γ-Fe as primary phase followed by an eutectic reaction forming γ-Fe + M_7C_3.

Figure 8 shows the D2 steel spray-formed billet, the microstructure of which was analyzed in a transversal cross section at 70 mm from the top. The porosity level in this case was also lower than 1 pct (in area fraction). Figure 9 shows microstructures of the D2 steel overspray powders, which present a refined dendritic microstructure with the M_7C_3 carbides in the eutectic constituent between the dendritic arms. The secondary dendrite arm spacing for the 50 μm droplet is around 1.5 μm. In contrast, the spray-formed billet presents an equiaxed grain microstructure (average grain size of 23.5 μm) with continuous M_7C_3 carbides around the grain boundaries (Figure 10). As previously observed in the case of boron modified supermartensitic stainless steel, no remnants of the dendritic microstructure of the droplets can be seen in the spray-formed microstructure. Although some round precipitates smaller than 1 μm can be seen in the middle of the austenitic grains, the continuous M_7C_3 carbides network (clearly seen in Figure 10(b)) suggests that most of the carbides were formed from the eutectic reaction of the last liquid present in the deposition zone. Figure 11 presents the surface temperature of the deposition zone measured in the spray-forming run of the D2 steel billet. One can see that the surface temperature during the deposition process is approximately constant at 1608 K (1335 °C). By observing the pseudo-binary phase diagram in Figure 7, it can be seen that this temperature lies within the γ-Fe + L field, which proves that the equilibrium temperature at the deposition zone is above the *solidus* temperature. When the deposition is finished

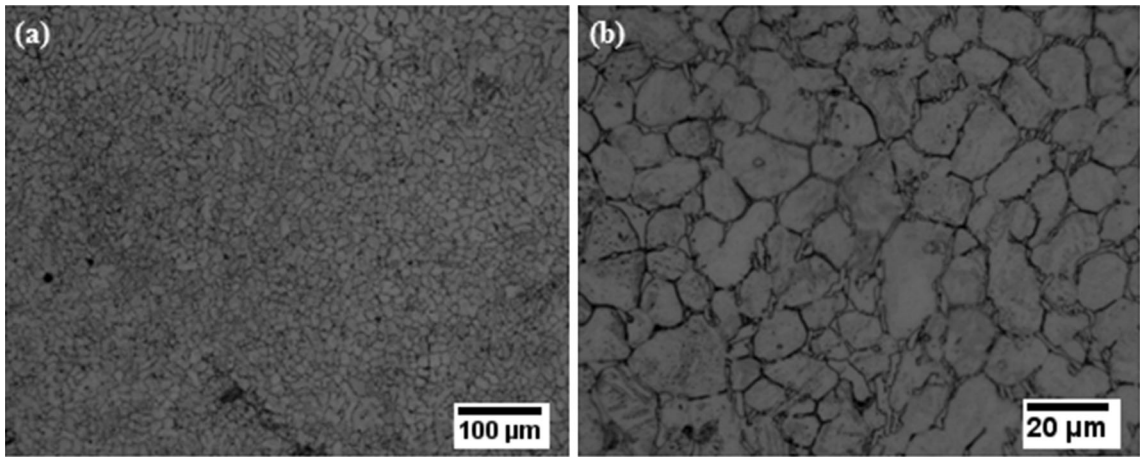

Fig. 4—Microstructure of the spray-formed SM-0.7B at two different magnifications.

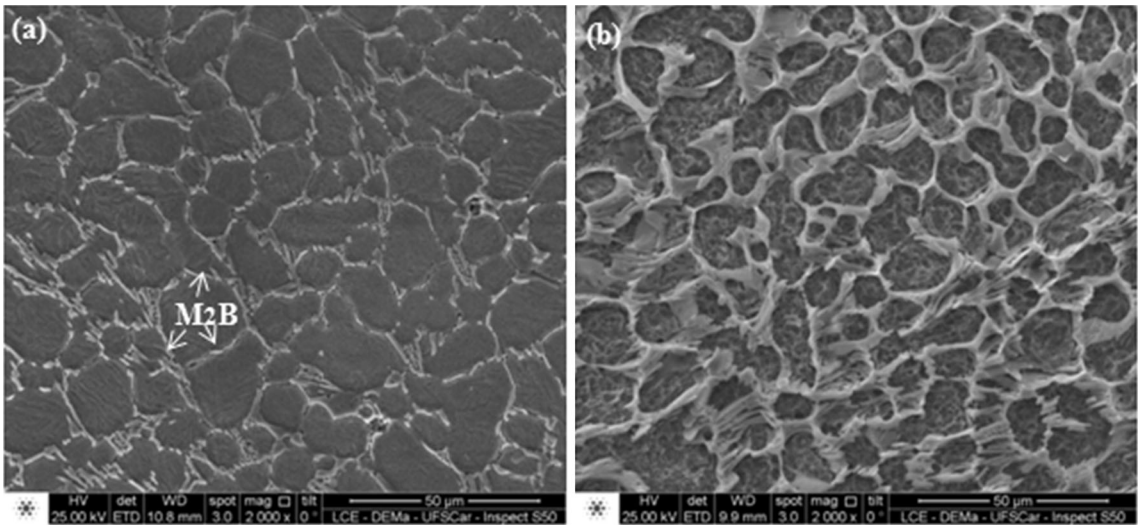

Fig. 5—SEM images showing (*a*) microstructure and (*b*) M_2B borides morphology (deep etching) of the spray-formed SM-0.7B.

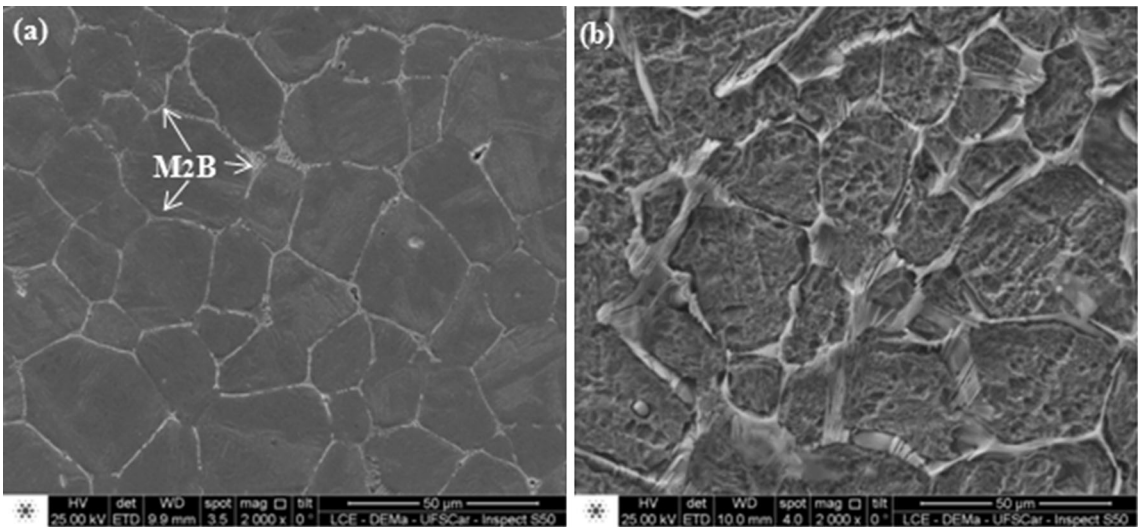

Fig. 6—SEM images showing (*a*) microstructure and (*b*) M_2B borides morphology (deep etching) of the spray-formed SM-0.3B.

the surface temperature drops sharply from 1608 K to 1298 K (1335 °C and 1025 °C) due to the gas flow on the deposit surface. However, when the gas flow is interrupted, the deposit surface cools down slowly at approximately 20 K/minutes. This result suggests that during the deposition process, the cooling rate must be slower than 20 K/minutes since hot droplets are continuously deposited, which is in accordance with what has been reported in the literature.[20,21]

C. *Solidification Model*

This paper proposes a model to explain the solidification sequence of steels, based on two main assumptions:

(1) When steady deposition is reached, the deposition zone has a constant temperature above the alloy's *solidus* temperature, which is approximately the surface temperature of the deposit during the deposition process. The deposition zone's temperature is strongly dependent on the processing parameters applied.
(2) The liquid and solid fractions in equilibrium are attained for the temperature of the deposition zone.

The model will be described considering the spray-forming of hypothetical A–B binary alloy with hypoeutectic composition X_0, as shown in the phase diagram of Figure 12. In this example, the solubility of B in the A-phase is nil.

When the deposition starts, a distribution of fully liquid, partially solidified, and completely solidified droplets impinge on a substrate (pre-heated or not). The liquid droplets spread across the substrate, drawing in the partially and totally solidified droplets and the deposit starts to build up. In the first stages of

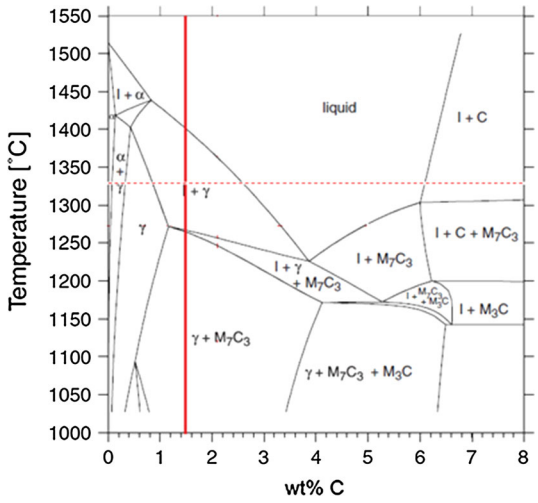

Fig. 7—ThermoCalc equilibrium simulations of pseudo-binary phase diagram varying the carbon content in 12 wt pctCr tool steels.[32]

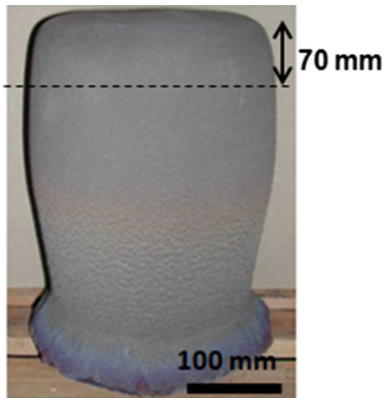

Fig. 8—D2 tool steel spray-formed billet. The dashed line shows the analyzed cross section.

deposition, the spray cone is still being stabilized and most of the heat in the droplets is transferred to the substrate. It was extensively reported that the non-stationary deposition conditions that occur at the initial stages of spray-forming lead to a microstructure with very high cold porosity (porosity caused if the fraction of liquid is too low and insufficient to fill the interstices between the solid particles in the deposition zone) in the vicinity of the substrate.[7,22] When the process reaches its steady-state condition, the deposit surface temperature remains constant and should be above *solidus* temperature to achieve a dense material. This model does not consider the transient deposition period and the microstructure evolution will be described from the point where the constant surface temperature is attained. At this point the completely solidified droplets with temperature T_{sd} (see Figure 12) reach the deposition zone with chemical composition X_0. Considering that these droplets continued under conditions close to equilibrium during solidification, the droplets microstructure is composed of X_0/X_e fraction of eutectic constituent and $1 - (X_0/X_e)$ fraction of primary dendritic A-phase. The partially solidified droplets with T_{psd} present only A-phase solidified and B-rich liquid phase with composition $X_{L,d}$. Figure 13 shows a schematic representation of the solidification model. When the droplets impact on the deposition zone the following sequence of events takes place:

(1) The fully liquid droplets spread, maintaining a liquid pool in the deposition zone. The completely liquid and partially liquid droplets cool down to $T_{surface}$ and the A-phase is solidified until the liquid fraction reaches the equilibrium fraction at this temperature. Meanwhile, the completely solidified droplets are heating up to $T_{surface}$ and the eutectic constituent and part of the primary A-phase is remelted or dissolved in the liquid present, until the equilibrium liquid fraction is attained. It is important to point out that the B element is now present only in the liquid since no solubility of B in the A-phase is possible.

(2) At this point, in the deposition zone only the A-phase embedded in a B-rich liquid is present. With the cooling of the deposition zone, the A-phase originally from the solidification of the liquid and partially liquid droplets and from the remaining solid phase after the partial remelting or dissolution of the solidified droplets, starts to grow. However, the continuous impacting of droplets induces a turbulent fluid convection and the liquid present in the deposition zone flows around the A-phase "nuclei". The movement of the liquid in the deposition zone plays two very important roles in the evolution of the microstructure: (1) chemical homogenization of the remaining liquid while solidification proceeds and (2) thermal homogenization of the remaining liquid, resulting in the gradient temperature around the A-phase "nuclei" being almost the same in all directions. The isotropic thermal gradient makes the "nuclei" grow without any preferential direction, which results in the development of equiaxed grains, following the Scheil-Gulliver model of solidification. As there is no solubility of B in A, the nuclei that are solidifying equiaxially will present the composition of A while the remaining liquid is enriched with B till eutectic composition is attained.

(3) When the remaining liquid reaches the eutectic temperature, all the liquid is solidified through the eutectic reaction at a constant temperature. When solidification is finished, the final microstructure is composed of equiaxed grains of A-phase with the eutectic constituent present at the grain boundaries around the primary A-phase.

An important aspect of this model is that when the equilibrium liquid fraction is attained, all the liquid present in the deposition zone is continuous. This means that the liquid from different droplets is mixed and that the solidification will be completed around the equiaxed A-phase with constant conditions for all pre-formed grains.

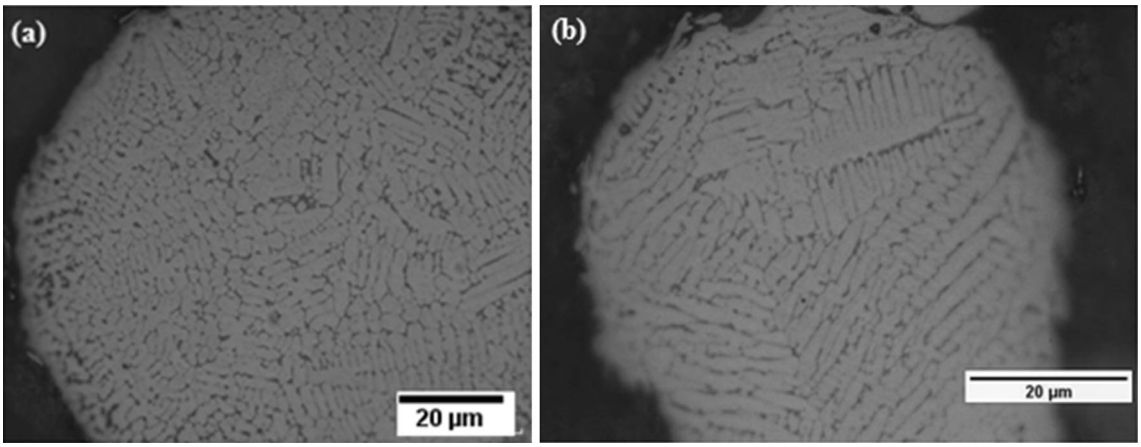

Fig. 9—Microstructure of the overspray powder of D2 tool steel with (*a*) 200 μm and (*b*) 50 μm.

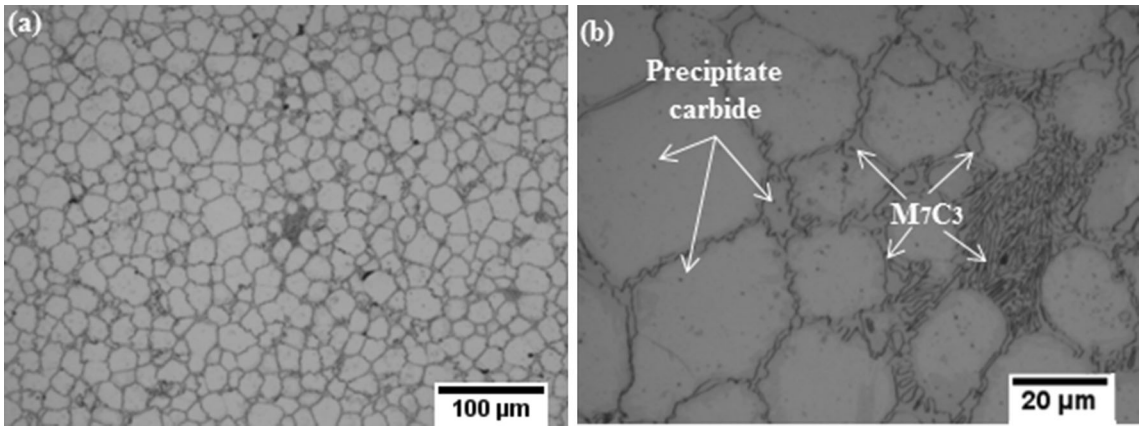

Fig. 10—Microstructure of the spray-formed D2 steel at two different magnifications.

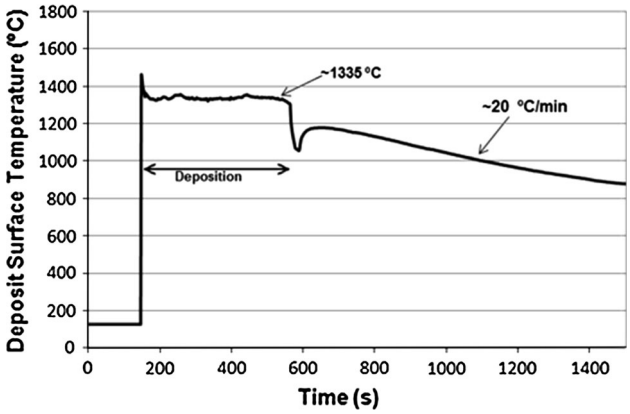

Fig. 11—Deposit surface temperature measured during the spray-forming process of the D2 tool steel billet.

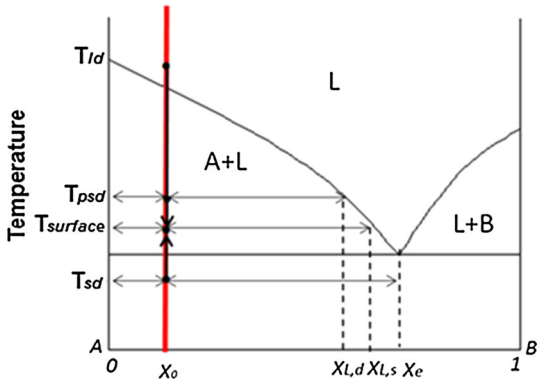

Fig. 12—Eutectic A–B binary phase diagram with no solubility of B in A and of A in B. T_{ld} = temperature of the fully liquid droplets; T_{psd} = temperature of partially solidified droplets; T_{sd} = temperature of completely solidified droplets; $T_{surface}$ = surface temperature of the deposition zone.).

III. DISCUSSION

It has been reported in the literature that spray-formed products with a low porosity level and high yield are achieved when the deposit surface temperature at the deposition zone is kept above the *solidus* temperature of the spray-formed alloy[7,22,23] This paper proposes a solidification model for spray-forming in which the equilibrium solidification path takes place in the deposition zone. Two cases of spray-formed products with low porosity and high homogeneity, processed in laboratory and on industrial-scale spray-forming equipments, have been used to support the proposed model.

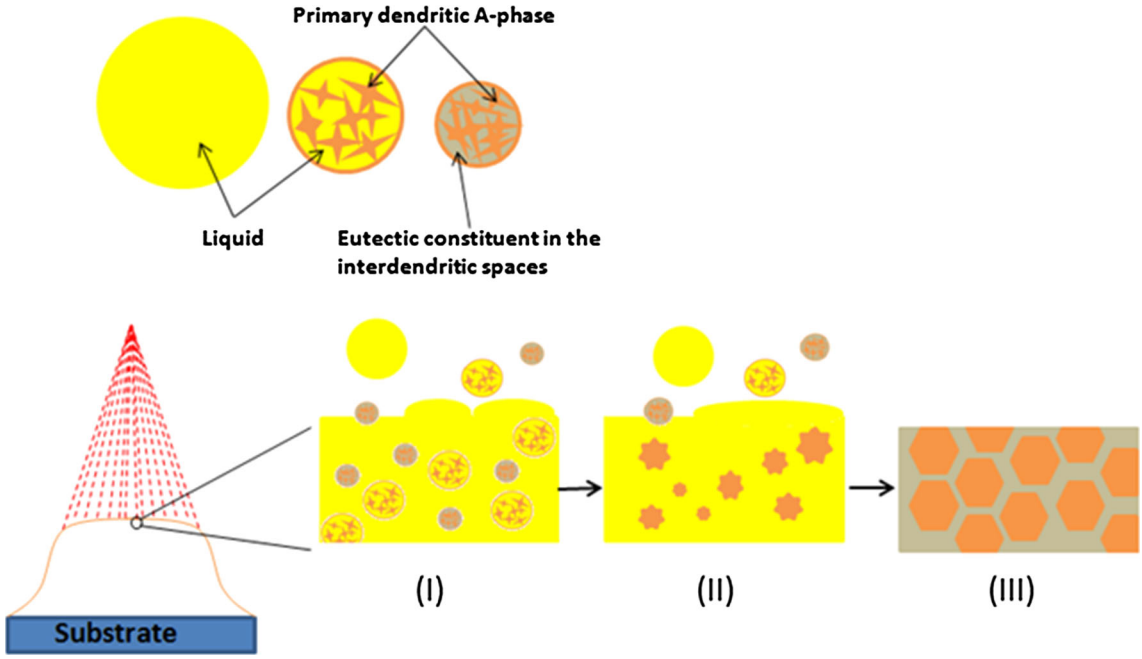

Fig. 13—Schematic representation of the solidification model.

The deposit surface temperature measurement during the spray-forming process of the D2 tool steel billet (Figure 11) clearly shows that for the full duration of the experiment, the deposition zone temperature is maintained constant and considerably above the *solidus* temperature. The proposed solidification model states that the solidified droplets, which land on the deposition zone, must be partially remelted and/or redissolved and that the equilibrium phase fractions at the deposition zone temperature must be attained. Such statement is well-supported by the disappearance of the very refined M_2B borides present in the completely solidified droplets, as observed in the overspray droplet microstructures, in the final spray-formed microstructure. Boron has very limited solubility in steel, which means that borides cannot be dissolved in the steel matrix. Thus, the only possible explanation for the disappearance of the borides present between the interdendritic arms (see Figure 2(b)) of the droplets, which are supposed to land completely solidified at the deposition zone, is by remelting and/or redissolving of this phase. This leads to an increase in the liquid fraction in the deposition zone. Observing the microstructure of the SM-0.3B and SM-0.7B spray-formed deposit, it is clear that all the borides were formed from the eutectic reaction when the liquid in the deposition zone reached the eutectic composition. Furthermore, the M_2B boride morphologies of the continuous eutectic network along the microstructures (Figures 5(b) and 6(b)) support the idea that the liquid in the deposition zone indeed must be continuous, and no "droplet regions" are preserved.

In the solidification model with A–B binary alloy (Figure 12), if a composition $X_1 < X_0$ is chosen, the equilibrium liquid fraction at the same $T_{surface}$ must be lower than in the case of the composition X_0. This means that for composition X_1 the primary A-phase nuclei must grow more during the cooling of the deposition zone, and a lower amount of liquid will reach the eutectic composition. Thus, the final microstructure expected for the composition, X_1, would be larger equiaxed grains and a lower fraction of eutectic at the grain boundaries when compared to the X_0 composition. This situation is well-represented by the different equiaxed grain sizes between the SM-0.3B and SM-0.7B, providing strong evidence that the austenite "nuclei" grow freely in the deposition zone until the remaining boron-rich liquid reaches the eutectic composition. This results in a much coarser grain size in the SM-0.3B than in the SM-0.7B. The equiaxed growth of the austenitic "nuclei" (considering here "nuclei" as being the remaining solid fraction of the particles that partially remelted) is attributed to the homogeneous gradient temperature in the deposition zone. The turbulent convection in the liquid present in the deposition zone, created by the constant impact of droplets, homogenizes both the temperature and the chemical composition. The same microstructure evolution was observed in the spray-formed D2 steel. Based on such results, it is stated that the solidification of steel in spray-forming occurs in conditions near equilibrium and, therefore, cannot be considered a rapid solidification process. Moreover, the high cooling rates prevailing during the atomization step do not contribute to the evolution of the spray-formed microstructure, since the rapidly solidified droplets are remelted and/or redissolved after being deposited. It has been reported that high cooling rates promoted by the atomization can lead to the formation of a primary phase with extended solubility.[24] In the case presented here, if the high cooling rates of the atomization step had led to formation of austenite supersaturated in boron, it would be expected that borides would precipitate within the

grains, since the cooling rate after the deposition process is quite slow. As no precipitates can be seen, there are two possible explanations: either (1) even with high cooling rates, the droplet solidification occurs in almost equilibrium conditions, and no extended solubility of boron in the austenite occurs; or (2) the high cooling rates lead to the formation of austenite with extended solubility of boron. However, when the droplets are partially remelted, the boron in the austenite "nuclei" diffuses back to the remaining liquid. This should be possible since the "nuclei" are considerably small (smaller than 10 μm) and the temperature in the deposition zone is sufficiently high to allow the diffusion of boron. The second explanation seems to be most likely to occur. In the case of D2 steel, since carbon has higher solubility in austenite than boron, some remaining carbon is present in the primary austenite, which leads to the precipitation of small round carbides, as shown in Figure 10(b). In any event, it is clear that the effects on the microstructure promoted by the rapid solidification of the droplets, in these cases, are not present in the final spray-formed microstructure. Thus, if the completely solidified droplets reach the deposition zone with phase fractions out of equilibrium, when remelted, the equilibrium phase fractions and compositions are restored, and the solidification sequence continues in near equilibrium conditions. However, the atomization step plays two very important roles in the evolution of the spray-formed microstructure: (1) the atomization supplies liquid droplets with very high chemical homogeneity to the deposition zone, which solidify in very small regions (hundreds or few micrometers[2]) avoiding macrosegregation; (2) the impacting of the droplets is essential to create the liquid convection in the deposition zone, allowing the primary nuclei to grow equiaxed.

It is worth stressing that the present solidification model in spray-forming is proposed to explain the solidification of steels with limited solubility of solute in the primary phase. Nevertheless, in cases where the solubility of the alloying elements is higher in the primary phase, for example, Cu-, Zn-, and Mg-containing Al-alloys, the effect of high cooling rates promoted during the atomization stage may be more preserved in the final microstructure, and other considerations should be made.[25] Several authors reported spray-forming as a rapid solidification process, in which it is possible to obtain extended solid solubility, metastable phases, and even amorphous phases.[17,26–31] Achieving such rapid solidification characteristics is indeed possible by spray-forming. However, the presence of rapid solidification features in spray-formed alloys is always accompanied by high cold porosity levels. In these cases, cold spray-forming conditions are applied, resulting in a deposition zone temperature under (or very close to) the alloy's *solidus* temperature, which allows the maintenance of the high cooled droplets' microstructure in the final deposit. When such cold conditions are applied, good quality spray-formed products are unlikely to be generated.

IV. CONCLUSIONS

A model for the solidification sequence of spray-formed steels based on near equilibrium conditions was proposed. The solidification model was supported and validated by microstructural analyses of boron modified supermartensitic stainless steels and D2 tool steel. The solidification model states that at the deposition zone following events take place:

1. During the deposition process, the temperature is kept constant and above the alloy's *solidus* temperature.
2. The liquid fraction of the fully liquid and partially liquid droplets is adjusted to the prevailing temperature until the equilibrium liquid fraction is attained.
3. The completely solidified droplets are partially remelted and/or redissolved until attaining the equilibrium liquid fraction.
4. The liquid is continuous and no "droplet regions" are preserved.
5. When cooled down from the equilibrium temperature, the liquid is solidified following the equilibrium solidification path.

ACKNOWLEDGMENT

The authors would like to thank the Brazilian institution FAPESP for its financial support.

REFERENCES

1. M.M. Pariona, C. Bolfarini, R.J. Dos Santos, and C.S. Kiminami: *J. Mater. Process. Technol.*, 2000, vol. 102, pp. 221–29.
2. P.S. Grant: *Prog. Mater Sci.*, 1995, vol. 39, pp. 497–545.
3. A. Schulz, V. Uhlenwinkel, C. Escher, R. Kohlmann, A. Kulmburg, M.C. Montero, R. Rabitsch, W. Schützenhöfer, D. Stocchi D. Viale: *Mater. Sci. Eng. A*, 2008, vol. 477, pp. 69–79.
4. C. Cui, A. Schulz, and V. Uhlenwinkel: *Materwiss. Werksttech.*, 2014, vol. 45, pp. 652–65.
5. J. Mi and P.S. Grant: *Acta Mater.*, 2008, vol. 56, pp. 1588–96.
6. J. Mi and P.S. Grant: *Acta Mater.*, 2008, vol. 56, pp. 1597–1608.
7. C. Meyer, N. Ellendt, L. Mädler, H. R. Müller, F. Reimer, and V. Uhlenwinkel, Materwiss. Werksttech., 2014, pp. 642–51.
8. N. Ellendt, V. Uhlenwinkel, and L. Mädler: *Materwiss. Werksttech.*, 2014, vol. 45, pp. 699–707.
9. L.A. Bereta, C.F. Ferrarini, C.S. Kiminami, W.J.F. Botta, and C. Bolfarini: *Mater. Sci. Eng. A*, 2007, vol. 448-451, pp. 850–53.
10. C.F. Ferrarini, C. Bolfarini, C.S. Kiminami, and W.J. Botta: F*Mater. Sci. Eng. A*, 2004, vols. 375–377, pp. 577–80.
11. H.A. Godinho, A.L.R. Beletati, E.J. Giordano, and C. Bolfarini: *J. Alloys Compd.*, 2014, vol. 586, pp. S139–42.
12. A.P.D.B. Guerra, N. Ellendt, V. Uhlenwinkel, P.S.C.P. da Silva, and C. Bolfarini: *Materwiss. Werksttech.*, 2014, vol. 45, pp. 568–73.
13. A.H. Kasama, A.J. Mourisco, C.S. Kiminami, W.J. Botta Fo, and C. Bolfarini: *Mater. Sci. Eng. A*, 2004, vols. 375–377, pp. 589–94.
14. C. Banjongprasert, S.C. Hogg, E. Liotti, C.A. Kirk, S.P. Thompson, J. Mi, and P.S. Grant: Metall. Mater. Trans. A Phys. Metall*Mater. Sci.*, 2010, vol. 41, pp. 3208–15.
15. E.J. Lavernia and Y. Wu: *Spray Atomization and Deposition*, 1st ed., John Wiley & Sons, Inc., New York, 1996, pp. 331–42.

16. P.S. Grant: Metall. Mater. Trans. A Phys. Metall*Mater. Sci.*, 2007, vol. 38A, pp. 1520–29.
17. H. Henein: *Materwiss. Werksttech.*, 2010, vol. 41, pp. 555–61.
18. N.J. Calos, E. Graham, D.R. Cousens, P. Christodoulou, C.H.L. Kennard, L.K. Bekessy, and S.F. Parker: *Mater. Trans.*, 2001, vol. 42, pp. 496–501.
19. P. Christodoulou and N. Calos: *Mater. Sci. Eng. A*, 2001, vol. 301, pp. 103–17.
20. K. Mingard, P. Alexander, S. Langridge, G. Tomlinson, and B. Cantor: *Acta Mater.*, 1998, vol. 46, pp. 3511–21.
21. C. Cui, U. Fritsching, A. Schulz, R. Tinscher, K. Bauckhage, and P. Mayr: *J. Mater. Process. Technol.*, 2005, vol. 168, pp. 496–504.
22. V. Uhlenwinkel and N. Ellendt: *Prog. Powder Metall. Pts 1 2*, 2007, vols. 534–536, pp. 429–32.
23. C. Kramer, V. Uhlenwinkel, and K. Bauckhage: *Solidif.*, 1998, vol. 1998, pp. 401–13.
24. A.V. Freyberg, M. Buchholz, V. Uhlenwinkel, and H. Henein: *Metall. Mater. Trans. B*, 2003, vol. 34B, pp. 243–53.
25. A. Hyodo, C. Bolfarini, and T.T. Ishikawa: Mater. Res*J. Mater.*, 2012, vol. 15, pp. 739–48.
26. C. Meyer, N. Ellendt, V.C. Srivastava, and V. Uhlenwinkel: *Int. J. Mater. Res.*, 2012, vol. 103, pp. 1090–95.
27. C.R. Afonso, C. Bolfarini, C. Kiminami, N. Bassim, M. Kaufman, M. Amateau, T. Eden, and J. Galbraith: *Scr. Mater.*, 2001, vol. 44, pp. 1625–28.
28. C.R.M. Afonso, C. Bolfarini, C.S. Kiminami, N.D. Bassim, M.J. Kaufman, M.F. Amateau, T.J. Eden, and J.M. Galbraith: *J. Non. Cryst. Solids*, 2001, vol. 284, pp. 134–38.
29. C.R.M. Afonso, C. Bolfarini, W.J.B. Filho, and C.S. Kiminami: *Mater. Sci. Eng. A*, 2007, vols. 448–451, pp. 884–89.
30. L.F. Bonavina, C. Bolfarini, W.J. Botta, E.R. D'Almeida, and C.S. Kiminami: *J. Alloys Compd.*, 2010, vol. 495, pp. 417–19.
31. C.S. Kiminami, W.J. Botta, and C. Bolfarini: *Materwiss. Werksttech.*, 2010, vol. 41, pp. 513–23.
32. D. Uhlenhaut, J. Kradolfer, W. Puttgen, J. Loffler, and P. Uggowitzer: *Acta Mater.*, 2006, vol. 54, pp. 2727–34.